QUANTIFYING THE SOIL FREEZING CHARACTERISTIC: THE DOMINANT ROLE OF SALT EXCLUSION

S. K. Amankwah[1,2], A. M. Ireson[1,2†], C. Maule[2], R. Brannen[2], S.A. Mathias[3]

[1]School of Environment and Sustainability, University of Saskatchewan, Saskatoon, 117 Science place S7N 5C8 Canada.

[2]Global Institute for Water Security, University of Saskatchewan, Saskatoon, 11 Innovation Boulevard S7N 3H5 Canada.

[3] Department of Engineering, Durham University, Durham, UK.

Corresponding author: Andrew Ireson (andrew.ireson@usask.ca)

† Current Address of corresponding author: Global Institute for Water Security, University of Saskatchewan, Saskatoon, 11 Innovation Boulevard S7N 3H5 Canada

Key Points:

- Cold regions hydrological models require quantification of the soil freezing characteristic relationship
- The Generalized Clapeyron Equation is found to under predict freezing point depression.
- A salt exclusion model and combined salt-capillary model perform well is simulating observed soil freezing characteristics

Abstract

The phenomenon of freezing point depression in frozen soils results in the co-existence of ice and liquid water in soil pores at temperatures below 273.15 K, and is thought to have two causes: i) capillary effects, where the phase transition relationship is modified due to soil-air-water-ice interactions, and ii) solute effects, where the presence of salts lowers the freezing temperature. The soil freezing characteristic curve (SFC) characterizes the relationship between liquid water content and temperature in frozen soils. Most hydrological models represent the SFC using only capillary effects with a relationship known as the Generalized Clapeyron Equation (GCE). In this study, we develop and test a salt exclusion model for characterizing the SFC, comparing this with the GCE-based model and a combined capillary-solute effect model. We test these models against measured SFCs in laboratory and field experiments with diverse soil textures and salinities. We consistently found that the GCE-based models under-predicted freezing-point depression. We were able to match the observations with the salt exclusion model and the combined model, suggesting that salinity is a dominant control on the SFC in real soils that always contain solutes. In modelling applications where the salinity is unknown, the soil bulk solute concentration can be treated as a single fitting parameter. Improved characterization of the SFC may result in improvements in coupled mass-heat transport models for simulating hydrological processes in cold regions, particularly the hydraulic properties of frozen soils and the hydraulic head in frozen soils that drives cryosuction.

Plain Language Summary

When the ground freezes during the winter, not all the water stored in the soil turns into ice, which is because soil particles hold tightly onto some of the water making it impossible to freeze the water and because of the presence of dissolved salts within the soil pore water. The presence of unfrozen water in frozen soils determines the hydraulic properties of the soil which are vital for models of flood forecasting during spring melt, snowmelt infiltration for crop growth and the mechanical properties that determine the stability of the ground for infrastructure in cold regions. In this study, we use laboratory and field experiments, as well as different theoretical models to understand the effect of either or both dissolved salt and soil particles on the amount of unfrozen water stored in the frozen soil, and we suggest that dissolved salts may often be the dominant control. We propose a new relationship for this phenomenon that could improve cold regions hydrological models.

1 Introduction

In cold regions, the way that ice and liquid water are held in the soil pore space plays a significant role in heat, solute and water transport (Spaans & Baker, 1996; He et al., 2016; Watanabe & Osada, 2017), which in turn influence winter evapotranspiration, snowmelt infiltration and runoff (Christensen et al., 2013; He et al., 2016), frost heave formation, thawing settlement, and frost depth penetration in frozen soils (Watanabe & Mizoguchi, 2002; Wen et al., 2012). Good knowledge of the properties of frozen soils is crucial in erosion control and flood risk

assessment during spring melt in cold climates. In engineering, information about these properties are employed in infrastructure development such as the construction of roads, pavements, airport runways, bridges and railway lines. Further, in agronomy, these properties are useful in understanding microbial metabolism (Oquist et al., 2009; He et al., 2016; Watanabe & Osada, 2017) and crop water uptake in frozen soils as well as estimating water requirements for winter crops.

Spontaneous processes, such as the phase change process, occur to minimize free energy. Ice (i) and liquid water (l) can co-exist only when they have equal free energy, and this occurs at 273.15 K (which is defined as T_0) for bulk water (Williams & Smith, 1989, p. 174, Zhang & Liu, 2018), where bulk water is defined as liquid water in an open container that is solute free and at atmospheric pressure. Above T_0, liquid water has lower free energy than ice, and therefore liquid water is the stable phase. When the temperature of pure free water drops below T_0, the free energy of the liquid phase becomes higher than that of the solid phase driving the transformation of liquid water into ice, and ice becomes the stable phase. Unlike bulk water, soil pore water is found to freeze progressively with temperature as the temperature drops below T_0 (Zhang & Liu, 2018; Hayashi, 2013; Williams & Smith, 1989, p. 175), a phenomenon termed *freezing point depression*. This was first recognized by Schofield (1935) who used theoretical relationships between sub-zero temperature and matric potential as a means to extend observed soil moisture characteristic curves into drier soil conditions, where tensiometers fail. Early empirical observations of freezing point depression were provided by laboratory experiments reported by Koopmans and Miller (1966) and Williams (1970). Freezing point depression is understood to occur because, in any individual soil pore, the effects of solutes and the attractive forces generated with the soil solids (capillarity and adsorption forces) reduce the free energy of the liquid water, such that the temperature must be less than T_0 for the phase transition to occur. Freezing point depression is therefore attributed to 1) capillarity and adsorption effects (hereafter capillary effects, Williams & Smith, 1989, p. 5; Spaans & Baker, 1996; Zhou et al., 2018), and 2) the presence of salts (Williams & Smith, 1989, p 5; Williams, 1970, p. 16; Williams, 1964; Watanabe & Mizoguchi, 2002). The freezing temperature of the depressed liquid water in any individual pore is defined as T_f, (K). Both capillary effects and salt exclusion effects result in progressive freezing, which is to say the water in the continuum of soil pore spaces has a distribution of freezing temperatures and freezing occurs progressively as the temperature drops below T_0. However, the reason these effects are both progressive are different. In terms of capillary effects, the capillary forces and thus the freezing point of the water in an individual pore depends upon the pore size (analogous to matric potential), so smaller pores have lower freezing temperatures (Spaans, 1994). In terms of salts, during freezing, salts are excluded from the ice leaving the remaining solution more concentrated, and thus the freezing temperature of the remaining liquid water is further depressed (Spaans & Baker, 1996; Williams, 1970, p. 17, Banin & Anderson, 1974).

Freezing point depression is quantified at the soil continuum scale through the soil freezing characteristic curve (SFC). The SFC relates the volumetric liquid water content, θ_l (-), to temperature, T ¿¿C), in frozen soils and is

analogous to the soil moisture characteristic curve (SMC), that relates liquid moisture content to matric potential, ψ (m) in unfrozen soils (Spaans & Baker, 1996; Flerchinger et al., 2006; Koopmans & Miller, 1966). The SFC can be directly measured for soils in the laboratory or the field by simultaneous measurements of liquid moisture content and soil temperature. Techniques to measure soil temperature include thermistors (e.g. Spaans & Baker, 1996; Stähli & Stadler, 1997; Bitelli et al., 2003), thermocouples (e.g. Tice et al., 1989; Flerchinger et al., 2006; Watanabe & Wake, 2009; Watanabe et al., 2011) and thermometers (e.g. Watanabe & Mizoguchi, 2002). Techniques employed in measuring the liquid water content include the use of dielectric sensors (Time Domain Reflectometry (TDR), Frequency Domain Reflectometry (FDR), and the Coaxial Impedance Dielectric Reflectometry) (Patterson & Smith, 1985; Bitelli et al., 2003; Watanabe et al., 2011; Susha Lekshmi et al., 2014; Zhou et al., 2014; Yao et al., 2016; Tian et al., 2017; Seyfried & Murdock, 2004; Kelleners et al., 2009; Kelleners & Verma, 2010; Kelleners & Norton, 2012; Francisca & Montoro, 2012), and the Neutron Magnetic Resonance technique (NMR) (Tice et al., 1982; Yoshikawa & Overduin, 2005; Watanabe & Wake, 2009; Tian et al., 2018). Dielectric sensors are often used to measure water content in unfrozen soils, and work because the dielectric constant of liquid water (~81), is distinct from that of air (~1) and soil solids (4-7) (Susha Lekshmi et al., 2014). The dielectric constant of ice is around 3 (West et al., 2007, Kelleners & Norton, 2012), meaning that the bulk dielectric constant of the soil remains dominated by that of the remaining liquid water as the soils freeze, and the ice is essentially invisible to the probe (which can be shown by sensitivity analysis using the dielectric mixing model, presented by Kelleners and Norton, 2012). Thus dielectic probes are useful for measuring the liquid water content of frozen soils (useful, for example, to characterize the SFC) but are not useful to measure the total water content (ice plus liquid water, useful, for example, for quantifying the water balance, see Gray and Granger, 1986 who used a two-probe density meter, similar to a neutron probe). Kelleners and Norton (2012) measured SFCs for a range of seasonally frozen soils in Wyoming using the Stevens HydraProbe (Stevens Water monitoring System Inc, 2007). The significant advantage of this instrument is that it simultaneously measures temperature and the bulk dielectric constant – thus directly measuring the SFC. The HydraProbe measures the impedance of a reflected electromagnetic signal propagated through the soil, which is related to the bulk dielectric constant of the soil (Francisca & Montoro, 2012). The measured bulk dielectric constant is then used to estimate the liquid water content through a calibration equation. The HydraProbe measures temperature using a thermistor embedded in the base plate of the sensor head (Seyfried & Murdock, 2004; Kelleners & Norton, 2012). Here, we will use the HydraProbes to measure SFCs in the field and in the laboratory.

Most models for the SFC that are used in coupled heat and mass transport models for frozen soils (e.g. Hansson et al., 2004, Dall'Amico et al., 2011, Painter & Karra 2014, Clark et al., 2015) are based on predicting the SFC from the SMC using the Generalized Clapeyron Equation (GCE, Williams & Smith, 1989, Kurylyk & Watanabe, 2013). GCE based models assume that in frozen conditions the temperature predicts an equivalent effective soil matric potential, from which the liquid water content can be obtained from the SMC relationship (Zhang & Liu, 2018; Mohammed et al., 2018; Teng, 2020), and hence temperature is related to liquid water content. The advantage of this method is that there are no free parameters associated with the GCE relationship. However, this approach only

represents capillary effects (Kurylyk & Watanabe, 2013) and does not account for the effects of solutes on the SFC (Azmatch et al., 2012). Given that real soils do contain solutes this would seem to be a limitation with GCE based models, however, the relative significance of solute effects and capillary effects is not well documented or understood (Watanabe & Mizoguchi, 2002). There are extensive SFC datasets in the literature, from early work by Koopmans and Miller (1966) and Williams (1970) through to recent experimental work by Schafer and Beier (2017), Ren and Vanapalli (2019), Ren and Vanapalli (2020) and Caicedo (2017), and including papers where the solute effects are quantified (e.g. Patterson & Smith, 1985, Zhou et al., 2018). To validate the GCE model requires both observed SFC and SMC data, which are not present in all of these studies. Both Williams (1970) and Koopmans and Miller (1966) present data that shows that for some soils the GCE predicted SFC is consistent with the observed SFC and for others is not, and they suggest that where the GCE fails it may be due to solutes. Koopmans and Miller (1966) found that the GCE works better for finer soils, and suggested that for non-clay soils, a correction factor for the ratio of interfacial tension between water and soils versus water and ice can be applied to improve the predicted SFC. Gharedaghloo et al. (2020) adopted this approach to successfully map the SMC onto the SFC for a series of laboratory experiments, and they used pore scale simulations to demonstrate the differences in ice-entry versus air-entry that this adjustment factor is designed to correct for. In contrast to this, Caicedo (2017) found that the GCE relationship fit SFC observations well for a fine sand and silt soil, while Ren and Vanapalli (2019) found that it did not fit observations well for two different clay soils. Spaans and Baker (1996) used a modified version of the GCE to account for osmotic potential (which the authors conclude is important at temperatures just below 273.15 K) and the temperature dependence of the latent heat of fusion. They suggest that their model matches observations, but they do not present SMC and SFC data independently, meaning that it is not clear how well the standard uncorrected GCE would perform. Schafer and Beier (2017) applied the Spaans and Baker (1996) model to a range of soils with mixed results, and suggest that limitations in performance maybe due to the presence of solutes. Zhou et al. (2018) extended the Generalized Clapeyron Equation to account for solute effects, and showed that their model was able to reproduce SFCs for saline soils from various laboratory experiments that were reported in the Chinese literature. In summary, the performance of the "standard" GCE model is mixed, and the instances where this model fails suggest it may not be a good model to adopt uncritically in coupled heat and mass transport models. Corrections that have been proposed for solutes or for differences in surface tension do not seem to work universally, and hence understandably have not been adopted in coupled models.

This study was designed to obtain both field and laboratory data that quantifies the SMC and SFC for different soil textures and salinities and to compare the results with those obtained from three different models: 1) capillary effects (the GCE approach); 2) salt exclusion effects; 3) combined capillary and salt exclusion effects.

2 Materials and Methods

2.1 Laboratory Experiments

The objective of the laboratory experiments was to measure the SMC and SFC of silica sand under controlled conditions. Silica sand was used with de-ionized water to give very low dissolved solutes in the pore water. The silica sand used was a fine-medium standard graded sand (ASTM C778 graded sand from Ottawa, Illinois Region, United States) with particle size ranging from 0.1 mm to 1 mm. The particle size was determined using the mechanical shaking method (Yan et al., 2017; Pekrioglu Balkis, 2019) with a set of sieves. The sand has a measured particle density of 2.5 g cm^{-3}, an estimated bulk density of 1.45 g cm^{-3}, and a porosity of 0.42. The particle density was measured using the pycnometer method as described by Pires et al. (2015), and the soil porosity was determined as the saturated volumetric moisture content of the soil. In both methods, adequate soil packing was achieved by carefully beating the sides of the soil container with a wooden meter rule until there was no change in the level of the sand in the container. If the level of the sand dropped, more sand was added, and the beating repeated. The bulk density of the sand was computed from the measured particle density and porosity.

The SMC of the sand was measured using the HYPROP set-up (UMS GmBH in Munich, Germany). The sand was repacked into the sampling ring of the HYPROP using the same packing techniques as described in the previous paragraph. Following soil packing, the sample was saturated by placing the sampling ring in a bowl of de-aired distilled water for 24 hours. After 24 hours, the sampling ring was removed from the bowl and placed on top of the sensor unit of the equipment. The soil was then allowed to dry by evaporation. Soil moisture content and matric potential were measured simultaneously by the HYPROP using a mass balance (with an accuracy of ±0.001 g) and two vertically offset tensiometers (has an accuracy of ±0.015 m) (Breitmeyer & Fissel, 2017), respectively. Soil moisture and matric potential measurements were automatically logged at different time intervals.

The SFC of the same sand was measured using a soil column with dimensions 20 cm (diameter) by 40 cm (height). The column was made from PVC pipe with one end glued on to an acrylic plexiglass using a waterproof JB weld Epoxy. The column was insulated at the side with two layers of single-faced fiberglass to minimize horizontal temperature propagation through the column. The top of the column was left open so that freezing would begin from the surface of the soil. The bottom of the column was not insulated, but the acrylic plexiglass seal at the bottom of the column was thick enough to prevent freezing from beneath the columns. The soil was prepared at two different target moisture contents, 0.05 m^3 m^{-3} and 0.24 m^3 m^{-3} by thoroughly mixing by hand the appropriate amount of oven-dried soil and de-ionized water in a 34 liters (l) plastic container. For the saline treatments, the appropriate mass of salt was weighed and dissolved completely in the appropriate amount of de-ionized water before missing with the soil. Sodium chloride salt (sodium chloride, crystalline from Fisher scientific) was used for this experiment. The total volume of soil (V_t), volume of water (V_w), target volumetric liquid moisture content (θ_l), mass of salt (m_s), bulk salt concentration ($c_b = m_S/V_t$) and pore water salt concentration ($c_s = m_s/V_w$) used for the freezing experiments are detailed in Table 1. The soil was then packed into the columns at 5 cm intervals and compacted with

the base of a 250 ml flat bottom flask. Three pre-calibrated Stevens HydraProbes were inserted vertically into the soil at 5 cm, 15 cm, and 30 cm depths in the columns. The Stevens HydraProbe was used because of three reasons 1) it was readily available 2) it can measure soil moisture content and temperature simultaneously and 3) it is the same instrument used in our field experiments. The Stevens HydraProbe measures soil moisture content using the dielectric method, which relates the measured dielectric constant to the moisture content through a calibration equation (calibration equation specified by the Stevens Water monitoring System Inc, 2007). At each soil depth, a probe was inserted vertically into the soil, and the soil was packed around it. The probes were numbered according to their position within the column (probe 1 at 5 cm, probe 2 at 15 cm, and probe 3 at 30 cm, all from the start of the tines of the probes which are about 5.8 cm long). This was to ensure that the same probe was used at the same depth every time the SFC was measured. Following the soil packing, the columns were covered with a polyethylene sheet to prevent evaporation and allowed to sit for two days for moisture to equilibrate in the columns. The columns were then placed in a freezer to measure the SFC. For every treatment, both the freezing and thawing curves were measured. For the freezing runs, the temperature of the freezer was set constantly at 268.15 K. The soil was allowed to freeze until the temperature of all the soil depths approached the freezer temperature or when the moisture content stayed constant. Afterwards, the temperature of the freezer was raised to and kept constant at 277.15 K for the soil to thaw. The thawing runs were terminated when all the soil depths reached a temperature greater than 273.15 K. Soil moisture content ($m^3\ m^{-3}$) and temperature data (K) were logged every minute using a CR 3000 series data logger from Campbell Scientific.

Table 1

Salt (NaCl) and water treatments used in the laboratory freezing experiment

Treatment	V_t(l)	θ_l($m^3\ m^{-3}$)	V_w(l)	m_S(g)	c_b(g l^{-1})	c_s(g l^{-1})
1	12.58	0.05	0.629	0	0	0
2	12.58	0.05	0.629	1.258	0.1	2
3	12.58	0.05	0.629	5.032	0.4	8
4	12.58	0.05	0.629	10.064	0.8	16
5	12.58	0.24	3.0192	0	0	0
6	12.58	0.24	3.0192	6.038	0.48	2

2.2 Field Experiments

The objective of the field study was to measure the SMC and SFC for different in situ soils with varying texture and salinity. The field studies were conducted at the St Denis National Wildlife Area (SDN) in the Canadian prairies (Bam et al., 2019; Bam & Ireson, 2019) and the Boreal Ecosystem Research and Monitoring Sites (BERMS) Old Jack Pine (OJP) site in the boreal plans ecozone in Saskatchewan (Ireson et al., 2015; Nazarbakhsh et al., 2020).

The SDN field site is located in the semi-arid, cold Canadian prairies ecozone about 40 km east (106° 5' 36" W, 52° 12' 34" N) of Saskatoon, Saskatchewan (Hayashi et al., 1998; Nachshon et al., 2014). The site is partly cropped with wheat, barley, and canola while the rest of the vegetation is a combination of native and introduced grasses (Hayashi et al., 1998, Bam et al., 2019). The site is characterized by an undulating hummocky topography (Hayashi et al., 1998; Nachshon et al., 2014; Bam et al., 2019) with silty stratified sediments and glacial tills (Hayashi et al., 1998; Nachshon et al., 2014; Bam et al., 2019). Soils at SDN can be high in salt, particularly sulphate salts (Nachshon et al., 2014). The site experiences mean annual precipitation (1967-1996) of 358 mm, of which 74 mm occurs as snow (November to April) (Budhathoki, 2018). The mean monthly temperature for the site is 258.45 K for January and February and 291.85 K for July and August (Bam & Ireson, 2019). At SDN, soil moisture data were measured on a transect with three soil profiles, namely upslope, mid-slope and downslope. In this study, however, only observation from the upslope profile is used. Data sets used in the SDN analysis include time series data of soil moisture content ($m^3\ m^{-3}$), soil temperature (K), and matric potential (m) at 5 cm, 20 cm and 50 cm depths. The soil moisture content and soil temperature were measured using Stevens HydraProbes from Campbell Scientific inserted vertically in the soil at the different soil depths. These HydraProbes are the same as those used in the laboratory experiments. The soil matric potential was measured using the 229 heat dissipation matric water potential sensor from Campbell Scientific.

The OJP site is located east of Prince Albert National Park in the southern Canadian Boreal Forest (104.69° W, 53.92° N), Saskatchewan, Canada (Nazarbakhsh et al., 2020). As the name implies, the OJP site is dominated by jack pine (*Pinus banksiana Lamb.)* with an understory of reindeer lichen (*Cladonin spp*.) (Barr et al., 2012; Nazarbakhsh et al., 2020). The soil at OJP is a well-drained sandy soil (Barr et al., 2012; Nazarbakhsh et al., 2020) with a water table depth of at least 5 m below the soil surface (Barr et al., 2012). The OJP site receives an average precipitation of 307 mm (Nazarbakhsh et al., 2020) . It is estimated that about 21 % to 31 % of the total precipitation at this site occurs as snow (Ireson et al., 2015, Nazarbakhsh et al., 2020). The site experiences a mean monthly temperature of around 263.15 K in January and 293.15 K in July (Nazarbakhsh et al., 2020). For the OJP site, soil moisture content and temperature data sets for different soil depths exist. However, in this current study, soil temperature data at 5 cm depth and moisture content data at the top 15 cm were used. The reason is that the soils at the OJP site do not freeze much below 15 cm, which could be because the trees and understory provide insulation that keeps the soil warm. This site also does not have matric potential measurements, which are needed for establishing the SMC. As such, SMC data set published by Cuenca et al. (1997) for the same field site was used in this study. Cuenca et al. (1997) measured moisture content using both the neutron probe (Campbell Pacific Nuclear 503 Hydroprobe) and the TDR. Soil matric potential was also measured using a combination of in situ tension disk infiltrometers and water retention data from the laboratory (measured using soil cores). These experiments are described in detail by Cuenca et al. (1997). The raw data points were extracted from the original plot using WebPlotDigitizer (Version 4.2) (Rohatgi, 2015).

2.3 Modeling

As noted earlier, two possible causes of freezing point depression in soils have been identified: i) capillary effects (capillarity and adsorption effects on the free-energy of the pore-water, which is related to the soil pore-size distribution); and ii) solute effects (the effect of dissolved salts on the freezing temperature of free water, independent of the soil pore-size distribution). In this study, models are applied to simulate the soil freezing characteristic curve assuming: 1) capillary effects alone; 2) salt exclusion effects alone; and 3) combined capillary and solute effects.

Note that here, the unit of temperature is always in Kelvin. The freezing temperature for free pure water at atmospheric pressure is denoted T_0 and has a value of 273.15 K. The freezing temperature of water in a specific part of the soil pore space is denoted T_f. For convenience, we plot SFC curves using the freezing point depression of soil water, denoted T_d and defined as

$$T_d = T_f - T_0 \tag{1}$$

2.3.1 Capillary Model

When two phases of a pure substance (e.g. water and ice) are in equilibrium with one another, the temperature and Gibbs free energy (expressed here on a per unit mass basis), G (J kg^{-1}), of each phase must be the same, though the pressures, P (Pa), may differ (for example consider liquid water and water vapour at the water-air interface in a capillary tube). When there is a change in temperature or pressure a new equilibrium state will be reached, again with identical T and G in each phase, such that the change in Gibbs free energy, dG must also be the same for each phase. The change in Gibbs free energy is given by (Williams & Smith, 1989, p. 186 and 190)

$$dG = -sdT + vdP \tag{2}$$

where s (J K^{-1} kg^{-1}) is entropy and v is specific volume (m^3 kg^{-1}). Hence for ice (subscript i) and liquid water (subscript l) we can write

$$v_l d\,P_l - v_i d\,P_i = (s_l - s_i)\,dT \tag{3}$$

During phase change, the change in entropy is due to the consumption or release of latent heat, so that (Williams & Smith, 1989, p. 190)

$$s_l - s_i = \frac{L}{T} \tag{4}$$

where L (J kg^{-1}) is the latent heat of fusion. Hence we have

$$v_l d\,P_l - v_i d\,P_i = \frac{L}{T} dT \tag{5}$$

Equation 5 is not controversial in the literature, but different assumptions have been made about how to deal with the ice pressure, P_i (Kurklyk and Watanabe, 2013). Here we will adopt the most common assumption for this (Hayashi, 2013, Williams & Smith, 1989, Hansson et al., 2004, Dall'Amico et al., 2011, Painter and Karra 2014, Clark et al., 2015) which is that there is no change in ice pressure, $d\,P_i = 0$. Noting that the density of water, ρ_l (kg m^{-3}) is equal to $1/v_l$, we have

$$\frac{d\,P_l}{dT} = \rho_l \frac{L}{T} \tag{6}$$

Matric potential, ψ (m), is defined from the relationship $P_l - P_a = \psi \rho_l g$, where g (m s^{-2}) is gravitational acceleration and P_a is atmospheric pressure, which can be treated as constant. Hence we have

$$\frac{d\psi}{dT} = \frac{L}{Tg} \tag{7}$$

Integrating this equation between $\left(T = T_0, \psi = 0\right)$ and $\left(T = T_f, \psi = \psi_f\right)$, we have

$$\psi_f = \frac{L}{g} \ln\left(\frac{T_f}{T_0}\right) = \frac{L}{g} \ln\left(\frac{T_0 + T_d}{T_0}\right) \tag{8}$$

Equation 8 is approximately equal to $\psi_f = L/g\left(T_d/T_0\right)$ (since $\ln\left(1+x\right) \approx x$, Kurylyk and Watanabe, 2013) i.e. a linear relationship between matric potential and temperature, that predicts a matric potential of -124m for a temperature of -1 K (Hayashi, 2013). Here we use non-linear form in Equation 8 since it will be important in our combined model below. If the soil is partially saturated at the time of freezing, the unfrozen matric potential, ψ_u (m), will be less than zero. Where ψ_u is the equivalent unfrozen matric potential, and is related to the total water content (ice plus liquid), which is not necessarily constant in frozen soil conditions (total water content changes due

to movement of liquid water, which can also refreeze in the soil and hence result in an accumulation of ice that the dielectric probes will not register). Ice will only form in the pore space when $\psi_f < \psi_u$. Hence, we have

$$\psi_l = \begin{cases} \psi_u & \psi_f \geq \psi_u \\ \frac{L}{g} \ln\left(\frac{T_0 + T_d}{T_0}\right) & \psi_f < \psi_u \end{cases} \quad (9)$$

Where ψ_l predicts the liquid water content, θ_l (m^3 m^{-3}), given here by the van Genuchten equation (VGN) (van Genuchten, 1980; Kelleners & Norton, 2012).

$$\theta_l = \theta_r + (\theta_s - \theta_r)\left(1 + (\alpha \psi_l)^n\right)^{-m} \quad (10)$$

where θ_r (m^3 m^{-3}) is the residual moisture content, and θ_s (m^3 m^{-3}) is the saturated moisture content or porosity, α (m¿¿−1)¿is approximately the inverse of the air entry matric potential, n and m are dimensionless empirical shape-defining parameters. Note that the total water content of the soil, θ_t (m^3 m^{-3}), ignoring changes in density of ice versus water, is given by

$$\theta_t = \theta_r + (\theta_s - \theta_r)\left(1 + (\alpha \psi_u)^n\right)^{-m} \quad (11)$$

and the ice content, θ_i (m^3 m^{-3}) is given by

$$\theta_i = \theta_t - \theta_l \quad (12)$$

Such that when $\psi_f \geq \psi_u$ then $\theta_t = \theta_l$ and $\theta_i = 0$.

Combining Equations 9 and 10 results in an SFC relationship between temperature and liquid water content, and this method describes the GCE model discussed in the introduction.

2.3.2 Salt Exclusion Model

In free-water saline solutions, the freezing temperature is depressed below T_0 due to the presence of solutes. Let T_m (K) represent the temperature below T_0 at which a saline solution of a given concentration will freeze (i.e. T_m is for salt exclusion what is T_d for the capillary model). Table 2 shows observed data from Haghighi et al. (2008) for salt concentration against freezing point depression for sodium chloride salt. Moreover, during freezing, salts are

341 excluded from the ice phase, making the remaining solution more concentrated, leading to a further depression in the
342 freezing point of the remaining liquid water (Banin & Anderson, 1974).

343 **Table 2**

344 *Freezing point depression for an aqueous NaCl solution. Here T_m (K) is the minimum temperature*
345 *below T_0 where only liquid water is present, for a given mass concentration of NaCl.*

Salt mass X (%)	1	5	10	15	18
$T_m(K)$	-0.58	-3.04	-6.79	-11.02	-14.29

346

347 X (%) is the mass fraction of salt in an aqueous solution such that

$$X = \frac{m_s}{m_w} 100 = \frac{c}{\rho_l} 100 \tag{13}$$

348 where m_s(g) and m_w(g) are the mass of salt and water, c(g l^{-1}) is the salt concentration, and the density of liquid
349 water here is expressed in units of g l^{-1} (i.e. ρ_l= 1000 g l^{-1}). c is thus given by $10X$. The relationship between
350 freezing point depression and salt concentration from Table 2 is well represented by a 2nd order polynomial function
351 passing through the origin,

$$T_m = p_1 c^2 + p_2 c \tag{14}$$

352 where T_m(K) is the minimum temperature below T_0 where only liquid water is present. p_1 and p_2 are found by
353 fitting Equation 14 to the observed data (Table 2) using linear regression. Following the fitting, the values of p_1 and
354 p_2 were found to be -0.00012544 and -0.05561807, respectively. Solving Equation 14 for c leads to

$$c = \frac{-p_2 - \sqrt{p_2^2 + 4 p_1 T_m}}{2 p_1} \tag{15}$$

355

356 Now, assuming that this relationship can apply to pore water within a soil control volume, V (l) with a fixed mass of
357 salt, m_s, then we have

$$c = \frac{\square_s}{(\square_l \square_r) V} = \frac{c_b}{(\square_l \square_r)} \tag{16}$$

where c_b(g l^{-1}) is the bulk solute concentration in the soil, i.e. mass of salt per soil control volume, m_s / V. Note that in Equation 16 we subtract the residual water content from θ_l which is equivalent to assuming that solutes are not freely exchanged between the free pore water and the residual water in the soil. We tested our models with and without this assumption and found that the predicted behavior of the model was more consistent with observed SFCs (which do not, normally, freeze to zero liquid water content) with this assumption. In our salt exclusion model, we assume that all of the pore water remains liquid until the temperature drops to T_m, corresponding to the solute concentration, c using Equation 14. As the temperature drops below T_m, the concentration of salt in liquid water increases according to Equation 15, and we find the liquid water content to sustain this concentration from Equation 16. Thus combining Equations 15 and 16 and substituting the maximum possible liquid water content in the soil, θ_m, for θ_l we have

$$\theta_m = \theta_r + \frac{2 c_b p_1}{-p_2 - \sqrt{p_2^{\,2} + 4 p_1 T_d}} \tag{17}$$

Equation 17 returns the maximum possible liquid water content for a given bulk solute concentration and soil temperature. The actual liquid water content, then, is given by

$$\theta_l = \begin{cases} \theta_t & \theta_m \geq \theta_t \\ \theta_m & \theta_m < \theta_t \end{cases} \tag{18}$$

Where again θ_t is the total water content corresponding to ψ_u. Equations 17 and 18 thus define an SFC relationship that predicts $\theta_l$based on the total water content (which can be given by Equation 11), soil temperature and the bulk soil solute concentration.

2.3.3 Combined Model

Models in the literature that combine the effects of solutes and capillary effects on freezing point depression do so by summing the osmotic and capillary potentials (Spaans & Baker 1996; Schafer & Beier 2017; Zhou et al., 2018). We instead assume here that the solute depression effect acts to lower the temperature at which freezing is initiated in the absence of capillary effects. Equation 7 (the GCE equation) is therefore integrated between the new limits $(T = T_m, \psi = 0)$ and $(T = T_f, \psi = \psi_f)$, thus giving

$$\psi_f = \frac{L}{g}\ln\left(\frac{T_f}{T_m}\right) = \frac{L}{g}\ln\left(\frac{T_0 + T_d}{T_m}\right) \tag{19}$$

The challenge we now face is that we have a circular problem: θ_l depends on ψ_f (Equation 10) which depends on T_m (Equation 19) which depends on c(Equation 14) which depends on θ_l (Equation 16). We therefore solve this problem using an iterative approach, as follows: for a given ψ_u, T and c_b we first guess the liquid water content θ_{l0}; next we use Equations 10, 19, 14 and 16 in sequence to calculate a new liquid water content, θ_{l1}; next we check the squared error $\left(\theta_{l0} - \theta_{l1}\right)^2$ against some tolerance value (10^{-8}) and if the error is too large we reset our initial guess to $\theta_{l0} = \omega\theta_{l1} + (1-\omega)\theta_{L0}$ and repeat these steps until convergence. Here ω is a relaxation factor (0-1) that is adjusted to improve the speed of convergence. Using this approach we were able to obtain stable convergence with $\omega = 0.05$. It is possible that an improved mathematical solution procedure could be obtained for this problem, but for our purposes, this approach is adequate.

2.3.4 Behaviour of the alternative models

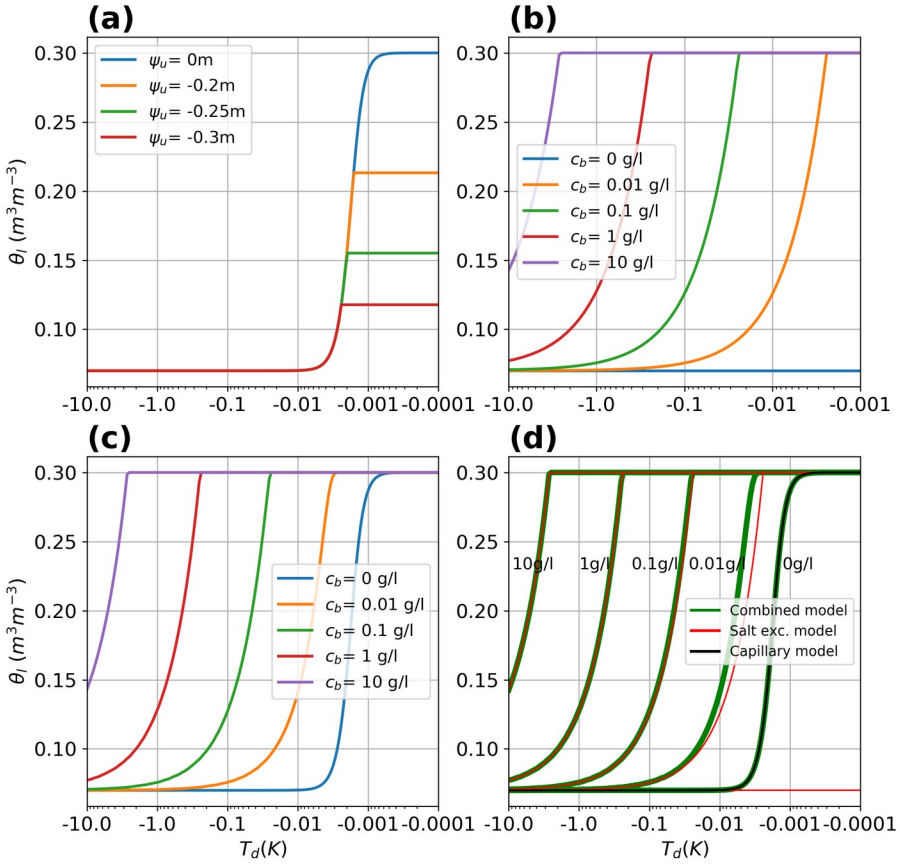

Figure 1. (a) Capillary model simulations with arbitrary soil parameters and differing ψ_u (or differing total water contents), (b) simulated results for the salt exclusion model using arbitrary parameters and differing salt mass (per bulk soil volume), (c) simulations for the combined capillary salt model (Equation 3.14) using arbitrary soil parameter and differing salt mass (per bulk soil volume), and (d) comparing the outcomes of the 3 models.

Table 3

Arbitrary soil parameters used in the model simulations

VGN parameters	Value
α (m^{-1})	-4.79
n	5
m	0.8
θ_{rv} ($m^3\ m^{-3}$)	0.07
θ_s ($m^3\ m^{-3}$)	0.3

The three models described above were run using arbitrary soil parameters (Table 3) to produce SFCs plotted in Figure 1. The capillary effect model (Figure 1a) describes the SFC for soils with no solute effects, and was run with different total water contents (represented using different equivalent unfrozen matric potentials ψ_u of 0 m, -0.2 m, -0.25 m and -0.3 m). The soil water remains liquid with reducing soil temperature until it reaches a certain depressed temperature when freezing commences, shown by the decrease in liquid water content with temperature. The salt exclusion model and combined model were both run for saturated conditions with changing bulk solute concentrations (c_b = 0 g l^{-1}, 0.01 g l^{-1}, 0.1 g l^{-1}, 1 g l^{-1}, and 10 g l^{-1}). The simulation results shows that the salt exclusion model (Figure 1b) predicts enhanced freezing point depression with increasing salt concentrations, or in other words, more liquid water remains at the same temperature for higher salt concentrations (represented by a shift of the curve to the left-hand side of the plot). This model simulates no freezing point depression if the solute concentration is zero – a condition that does not occur in real soils. The combined model (Figure 1c) behaves the same as the salt exclusion model at high solute concentrations, and the same as the capillary model with zero solute concentration, as would be expected. For the arbitrary soil that these simulations were run for, the salt exclusion model and combined model only differed noticeably when the solute concentration was less than 0.1 g l^{-1} (Figure 1d).

3 Results and Discussion

3.1 Laboratory Experiments

The observed SMC for the silica sand that was measured in a laboratory drying experiment, as described in section 2.1, is shown in Figure 2. The van Genuchten model (VGN) was fit to these data. The observed data did not extend up to saturation (i.e. $\psi_u = 0$) which is probably because the soil was not completely saturated at the start of the experiment. The saturated moisture content (θ_s) was set to be equal to the measured porosity of the soil (0.42 m^3 m^{-3}) The residual moisture content (θ_r) was identified visually from Figure 2. The parameters n, m, and α (Table 4) were obtained by optimization, minimizing the root mean squared error (RMSE) in water content. After fitting the RMSE was 0.017. The green dots are observed data points from the start of the experiment and were excluded from the fitting because they were not consistent with a typical SMC curve. This was likely due to non-equilibrium conditions in the soil sample at the beginning of the experiment. Judging from the results (Figure 2), this soil has poor water retention, and drains rapidly as the matric potential drops below about -0.1 m. The soil reaches its residual moisture content (about 0.02 m^3 m^{-3}) at a matric potential of about -0.38 m. This result is typical of coarse textured soils that lose moisture rapidly due to their large pore sizes.

SFCs measured in the laboratory for the same sand and with varying pore-water dissolved salt (NaCl) concentrations are plotted in Figure 3 (at a target moisture content of 0.05 m^3 m^{-3}) and Figure 4 (at a target moisture content of 0.24 m^3 m^{-3}). The results show, as expected, that higher salinity results in enhanced freezing point depression (curves

shift to the left), or in other words, for the same temperature more liquid water is retained in the soil at higher salt concentrations. The results also reveal the phenomenon of supercooling during freezing (depicted by the red-colored ring in the third plot on the third row of Figure 3a). The temperature of the soil decreased to what is termed as the temperature of spontaneous nucleation (T_{SN} ¿(Kozlowski, 2009; Zhou et al., 2020) without a change in moisture content. Supercooling is a metastable stage in freezing and is common in laboratory experiments. T_{SN} is the temperature at which a stable ice nucleus for ice crystallization forms in a freezing soil (Kozlowski, 2009). After reaching the T_{SN} there is a release of latent heat that warms the soil to its freezing point where freezing begins (Kozlowski, 2009; Ren & Vanapalli, 2020; Zhou et al., 2020). The supercooling effect is absent in the thawing curves (Figure 3b and 4b), which is as expected. Depicted in the purple ring (first plot on the first row of Figure 4a) is possible evidence of moisture migration during soil freezing. Here the liquid moisture increased with decreasing soil temperature. This observation may be due to the migration of moisture from unfrozen layers toward the freezing front, a phenomenon termed cryosuction. Experiments of Mizoguchi (1990), as described in Hansson et al. (2004) revealed the same phenomena during soil freezing. According to Hansson et al. (2004), this is due to the high hydraulic gradient established in the soil during freezing which causes moisture to move upwards toward the freezing front.

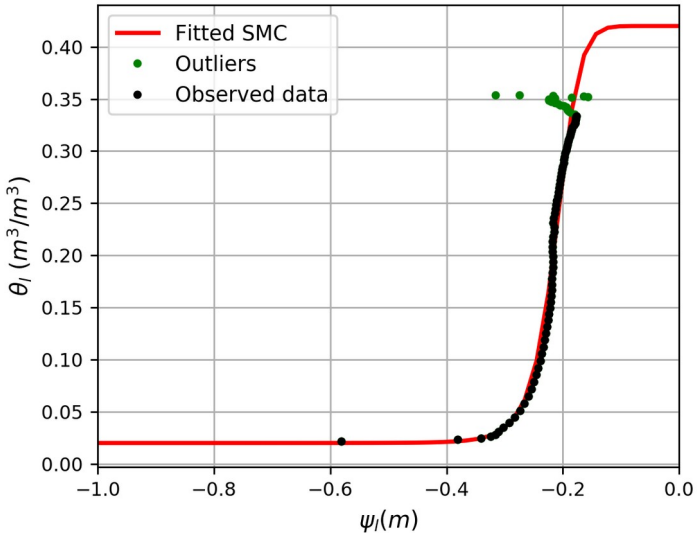

Figure 2. The soil moisture characteristic curve of silica sand measured using the HYPROP apparatus (black dots) and fitted to the van Genuchten model (solid red line)

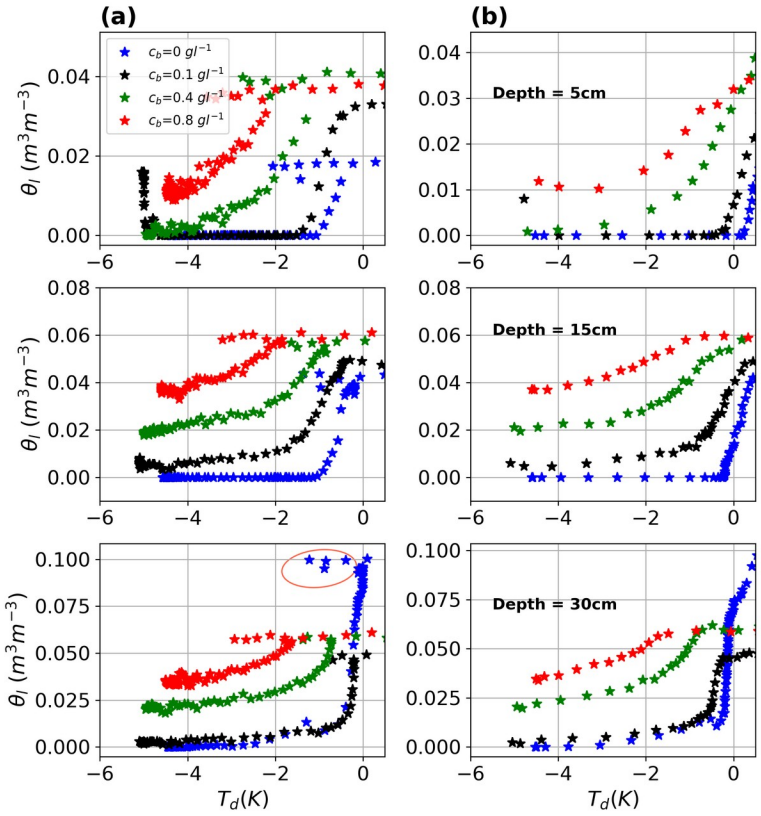

Figure 3. SFCs of the silica sand at different salt concentrations at a target moisture content of 0.05 m^3 m^{-3} (a) freezing curves for different soil depth, and (b) thawing curves for different soil depth

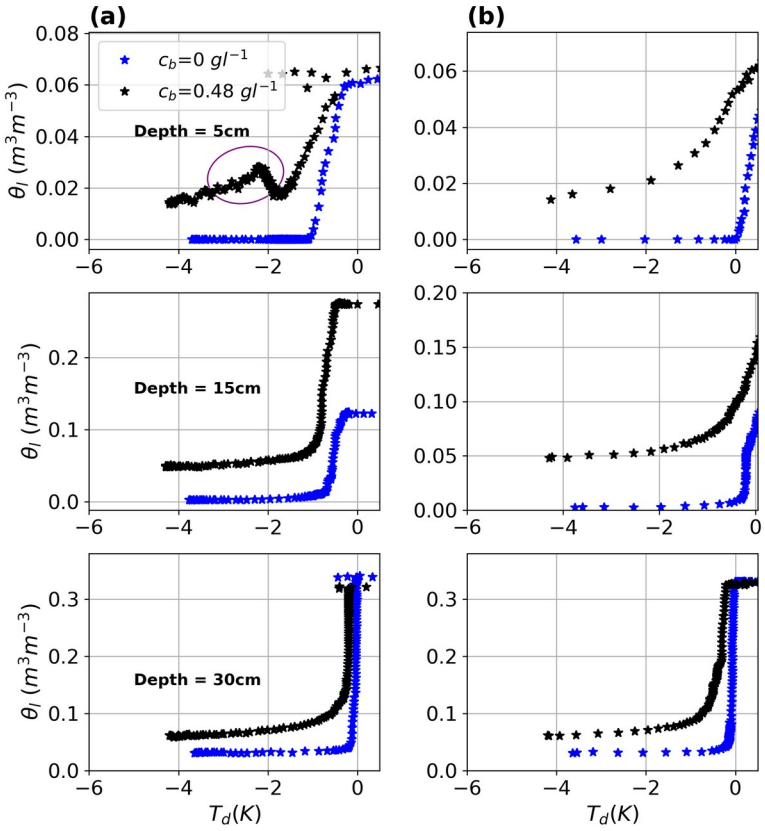

Figure 4. SFCs of the silica sand at different salt concentrations at a target moisture content of 0.24 m^3 m^{-3} (a) freezing curves for different soil depth, and (b) thawing curves for different soil depth

Table 4

Fitted parameters and RMSE for the SMC of the silica sand

VGN parameters	Value
α (m^{-1})	-4.79
n	10.11
m	0.90
θ_{rv} (m^3 m^{-3})	0.02
θ_s (m^3 m^{-3})	0.42

3.2 Field experiment

Figure 5 is the results for the SDN site: SMCs fitted to the VGN model (solid pink line) (Figure 5a), freezing curves (Figure 5b) and thawing curves (Figure 5c). The results show that the SMCs for the different years are different. Some specific reasons for this observation may include 1) shrinking or swelling of the soils, particularly because the soil here is rich in clay, and 2) the shifting of measuring instruments. The 2013 curves are used in all analysis, since the 2013 curves are wetter than the other years and looks reasonably consistent at all the soil depths. The curves were fitted to the VGN model by minimizing the root mean square error (RMSE), which is calculated from the difference between the observed moisture content and the predicted moisture content from the VGN model (fitting parameters values are documented in Table 5). The results also shows that the total water content at the onset of freezing (Figure 5b) was significantly lower than the total water content at the end of the thawing (Figure 5c). The pre-freeze up water content depends on how much rainfall fell in the late summer or fall months. The post thaw water content depends on moisture migration to the frozen soil over the winter months (cryosuction, which we cannot directly observe, since this water would refreeze and as ice it would be invisible to the dielectric probes), and infiltration of snowmelt that occurs before the soil thaws. The SMC of the OJP site and the VGN model (red line) is shown in Figure 6a (find parameter values in Table 6). Similar to the laboratory soil, the OJP soil is coarse-textured and loses moisture rapidly. Again, we see here that the thawing curve (Figure 6c) ends up wetter than the freezing curves (Figure 6b), which we attribute solely to snowmelt infiltration. The OJP site has very low moisture content; hence moisture migration may not be practical.

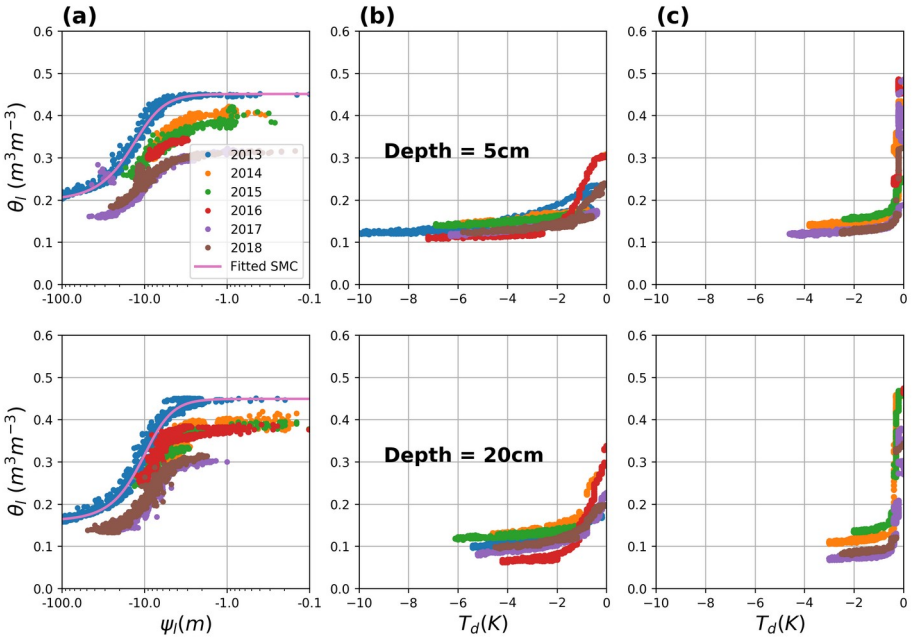

Figure 5. Results for the SDN field site; (a) SMCs for different years fitted to the van Genuchten model (solid purple line), (b) freezing curves for different years, and (c) thawing curves for different years.

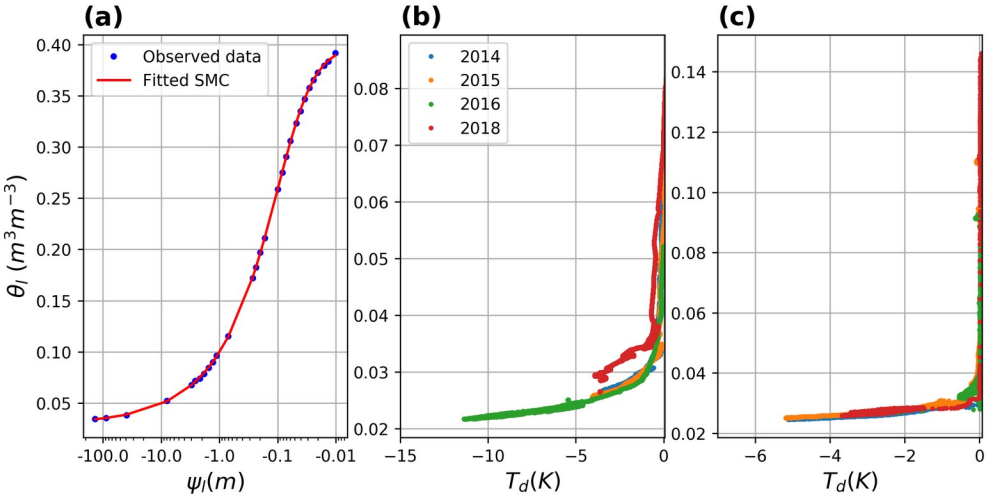

Figure 6. Results for the OJP field site; (a) SMC fitted to the van Genuchten model (solid red line), (b) freezing curves for different years for the top 15 cm depth, and (c) thawing curves for different years for the top 15 cm depth.

503 **Table 5**

504 *Fitted parameter values of VGN for SDN site*

505

Soil depth	Year	α (m^{-1})	n	m	θ_r ($m^3\ m^{-3}$)	θ_s ($m^3\ m^{-3}$)	RMSE
5 cm	2013	0.094	2.55	0.61	0.198	0.45	0.0095
20 cm	2013	0.12	2.72	0.63	0.16	0.45	0.0119
50 cm	2013	0.094	2.55	0.61	0.198	0.45	0.0095

506

507

508 **Table 6**

509 *Fitted parameter values of VGN for OJP site*

510

Parameter	α (m^{-1})	n	m	θ_r ($m^3\ m^{-3}$)	θ_s ($m^3\ m^{-3}$)	RMSE
value	19.44	1.6	0.4	0.03	0.4	0.00076

511

512 ## 3.3 Model performance

513 Models were run for each of the laboratory and field experiments, to reproduce the SFCs. We found that in many
514 cases, the residual water content, θ_r, was lower for the freezing curves (SFCs) compared with the drying curves
515 (SMCs). This could be an artifact of the probe, but we suspect that this could be a real phenomenon. This suggests
516 that the minimum pore size for drying is larger than the minimum pore size for freezing. Because of this, we
517 adjusted θ_r for our models to match the SFC data.

518

519 The validation results for the three models (capillary, salt exclusion and the combined model) using laboratory
520 measured SFCs are presented in Figure 7 and Figure 8. Here the models were compared with observations from 30
521 cm depth because the shallower probes (5 cm and 15 cm depths) froze rapidly and were possibly not in
522 thermodynamic equilibrium, and hence may overpredict the freezing point depression in the soil. The bulk soil salt
523 concentrations were assumed to remain constant for the duration of the experiment, i.e. we ignore any potential salt
524 redistribution in the soil profile.

525

526 Figure 7 presents the results for the case where no salt was added to the soil in the experiment. In Figure 7a, a value
527 of $c_b = 0$ is used in the salt exclusion and combined models, and the performance of the three models are compared.
528 As expected, the capillary and combined models are identical and the salt exclusion model predicts no freezing point
529 depression. The performance of the capillary model is poor, which suggests that the assumptions within the GCE are

530 inappropriate for this soil. Despite our efforts to minimize solutes (using de-ionized water and pure silica sand), the
531 soil pore water may still contain some amounts of dissolved salts, that may result in higher depression of the
532 freezing point in the SFCs. This was tested by mixing 100 g of sand with 100 ml of deionized water and measuring
533 the electric conductivity (EC) after the mixture was stirred for about 5 minutes and allowed to settle. A calibrated
534 conductivity meter gave a reading of 19 μS cm^{-1}, equivalent to $c_b = 0.024$ g l^{-1} (the EC was converted to c_s, i.e.
535 TDS, by multiplying by 0.64, Chang et al., 1983). Note that this is just an estimate of the salt concentration in the
536 sand since the actual conversion of EC to TDS depends on the activity of the different ions in the sand. When this
537 concentration was used in the combined and salt exclusion models their performance was markedly improved,
538 Figure 7b, though the model still did not fit the observations. These models could be made to fit the observations
539 well by using a value of $c_b = 0.12$g l^{-1}, Figure 7c, determined by manual calibration. This is likely an unrealistically
540 high solute concentration for this experiment. It must be noted that the temperature in Figure 7 is on a log-scale, and
541 the errors in Figure 7a and b are smaller than the reported error tolerance of the temperature observations with the
542 probe (± 0.3 K).
543
544 The results for the experiments where a fixed mass of NaCl salt was added to the soil are shown in Figure 8. The
545 poor performance of the capillary model was unchanged, but both the salt exclusion and the combined model
546 performed well without calibration or refinement. Since the predictions from the combined and salt exclusion
547 models were identical, this implies that the SFCs here are completely dominated by the salt exclusion effect.
548

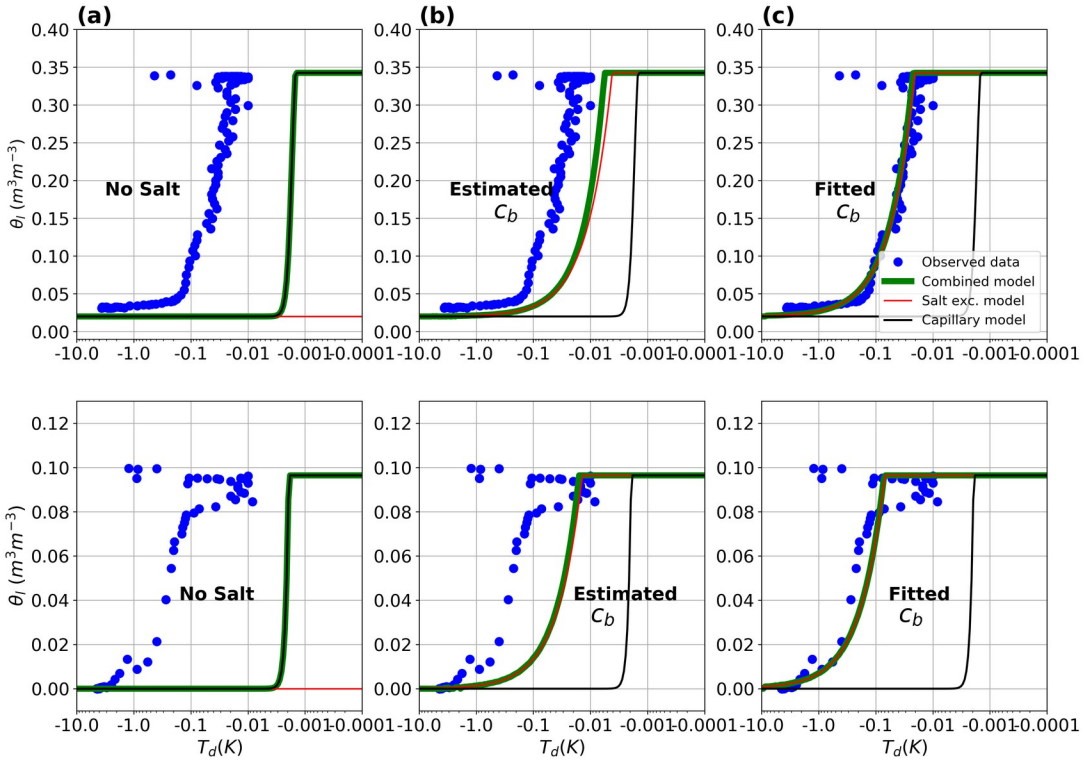

Figure 7. Performance of the three models (capillary, salt-exclusion and combined model) against laboratory observed SFCs at 30 cm depth with no salt added: (a) salt exclusion and combined models with no fitting, $c_b = 0$ g l^{-1}; (b) salt exclusion and combined models with estimated $c_b = 0.024$ g l^{-1} and (c) salt exclusion and combined models fitted to the data with $c_b = 0.12$g l^{-1}. Upper panel is results for higher antecedent moisture content and lower panel is results for lower antecedent moisture content.

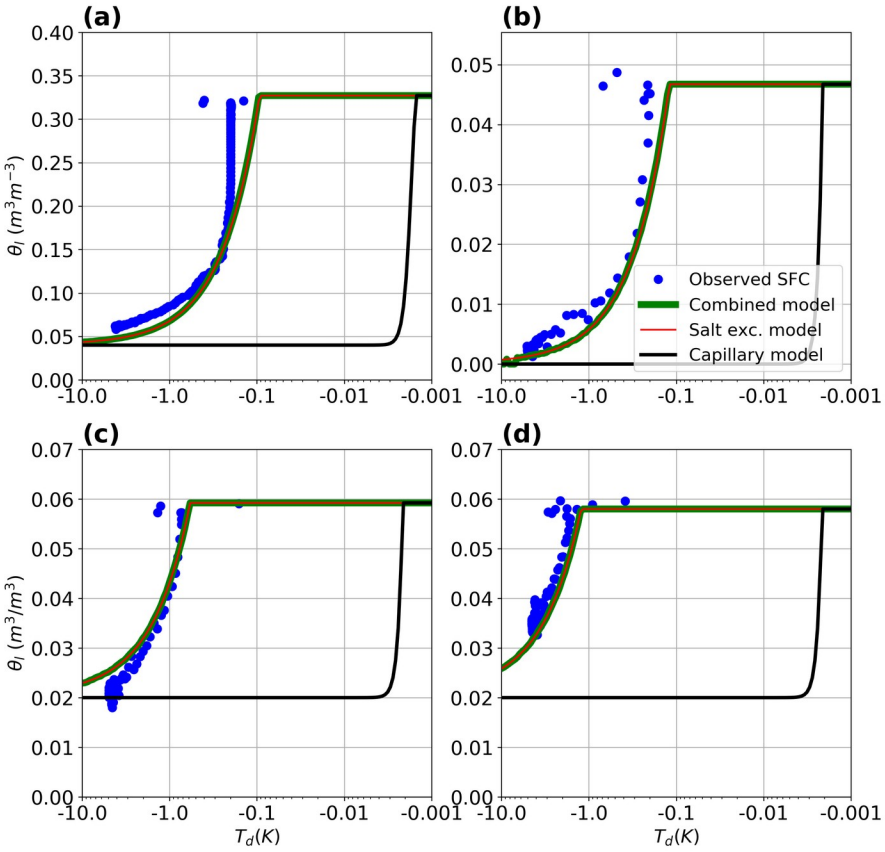

Figure 8. Performance of the three models (capillary, salt-exclusion and combined models) against laboratory observed SFCs at 30 cm depth for different salt concentrations and water contents: (a) c_b=¿0.48 g l^{-1}; high moisture content (b) c_b=¿0.1 g l^{-1} ; low moisture content (c) c_b=¿0.4 g l^{-1} ; low moisture content, and (d) c_b=¿ 0.8 g l^{-1}; low moisture content.

Figure 9 and Figure 10 show the performance of the three models at the SDN and OJP field sites, respectively. The models were first run without salt ($c_b=0$,Figure 9a and Figure 10a) and then by adding arbitrary amounts of salt to fit the models to the observed SFCs (Figure 9b and 10b). Note that at SDN the largest adjustments to θ_r were made, and it is clear from the observations alone (Figure 5) that there are significant differences in the lower limit of the liquid water content for drying and freezing. The model results show that for both field sites (SDN and OJP), the capillary model and the identical combined model with zero salt underestimated freezing point depression (Figure 9a and 10a). This is less surprising than for the laboratory experiments because we expect significant amounts of dissolved salts in these field soils. The underestimation is smaller at the OJP site (Figure 10a) than at the SDN site (Figure 9a), which was also expected because the OJP site has less saline soil, and thus, the salt exclusion effect

should be smaller. Again, the salt exclusion model failed as expected when no salt was added to the model. In Figure 9b and 10b salt was added to the model to fit the observed SFCs, and here both the salt exclusion and the combined model did well in predicting the observed SFCs for both field sites (Figure 9b and 10b). Comparing the average salt concentration used in the fitting run for the SDN site to those used at the OJP site (Table 7), we see that the SDN site has more salt than the OJP site, which is correct.

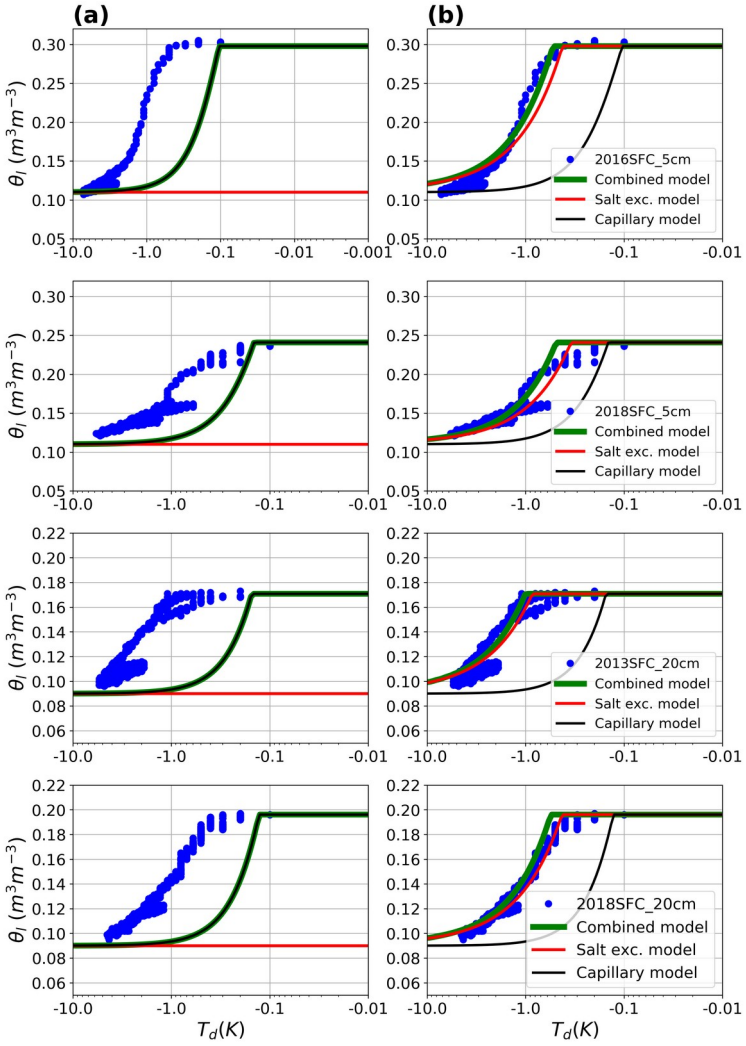

Figure 9. Performance of the three models (capillary, salt-exclusion and combined capillary salt model) against observed SFCs for SDN site; a) models applied without salt and, b) model fitted to the observed SFCs by adjusting the salt masses.

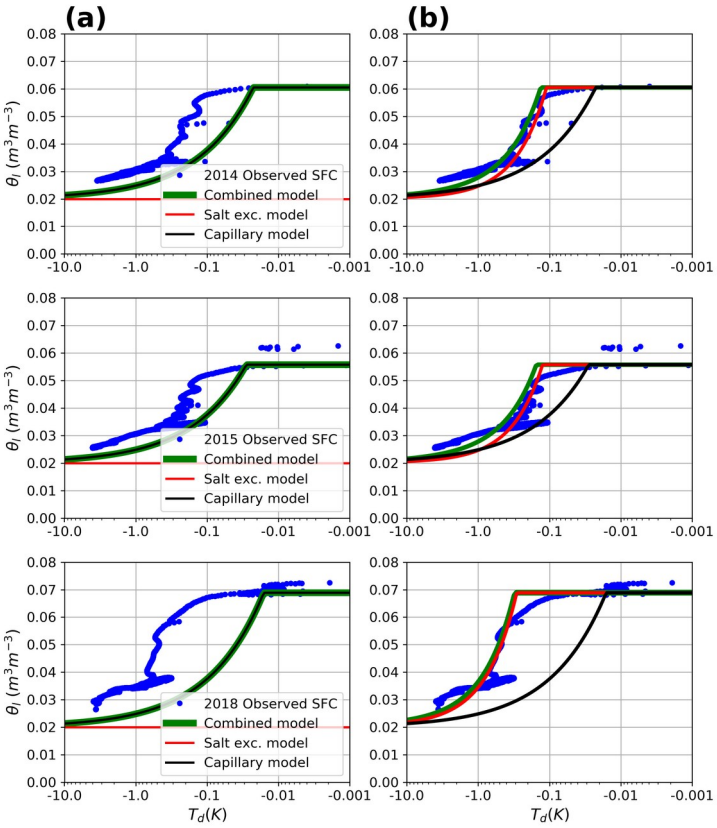

Figure 10. Performance of the three models (capillary, salt-exclusion and combined capillary salt model) against observed SFCs for OJP site ; a) models applied without salt and, b) model fitted to the observed SFCs by adjusting the salt masses.

Table 7

Bulk salt Concentration (c_b) used in the fitting runs for the SDN and OJP field sites

SDN site		OJP site	
Year and depth	c_b (g l^{-1})	Year	c_b (g l^{-1})
2016 5cm	1.4	2014	0.08
2018 5cm	0.8	2015	0.08
2013 20cm	1.2	2018	0.25
2018 20 cm	0.8	-	-
Average	1.05	Average	0.14

4 Conclusions

In this study, SMCs and SFCs were measured for soils with varying texture and salinity in laboratory and field conditions, using dielectric impedance probes to measure the liquid water content. In our seasonally frozen field sites, SFCs have a number of important characteristics, which we summarize conceptually in Figure 11, and describe here: *i)* the antecedent water content prior to freezing are normally not saturated, and may in fact be quite dry, meaning that assuming saturated soils for frozen conditions is likely to introduce significant errors; *ii)* the freezing and thawing curves are distinctly hysteretic (consistent with previously reported curves from Koopmans and Miller, 1966, Tice et al., 1989, and Watanabe and Osada, 2017); and *iii)* the soils are wetter, and perhaps saturated, at the end of thawing, which is due to a combination of possible soil moisture redistribution by cryosuction during the winter, and snowmelt infiltration during the melt period.

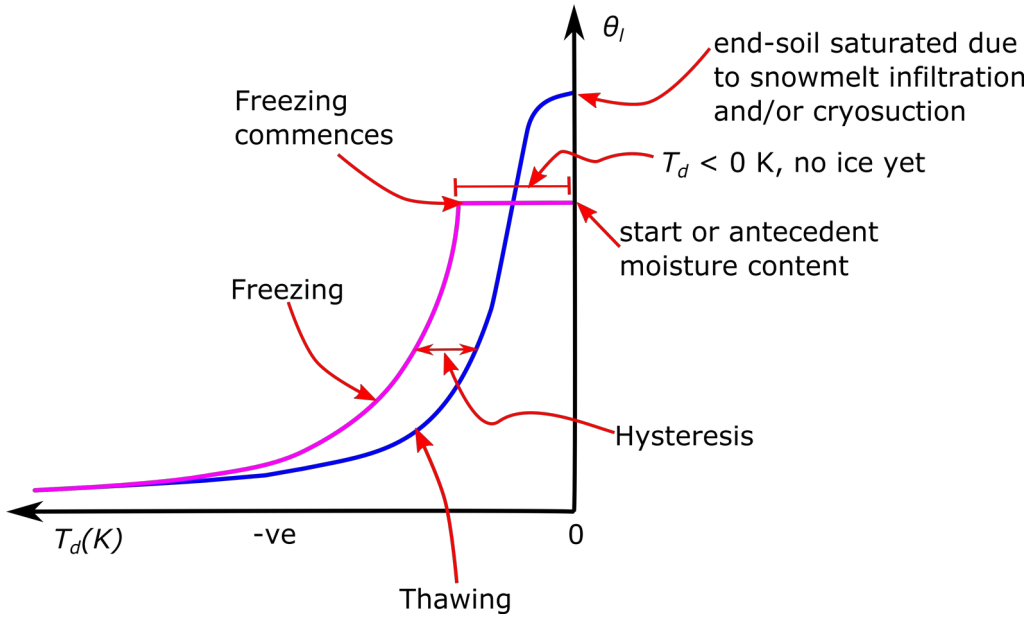

Figure 11: Conceptual diagram depicting the difference between freezing and thawing in frozen soils

Three alternative models were developed to simulate the SFC: a capillary model, based on the GCE; a salt exclusion model; and a combined model. The combined model is identical to the capillary model when there is no salt in the soil, and identical to the salt exclusion model when salt concentrations are high. The salt exclusion model fails to predict any freezing point depression when there is no salt in the pore water (though such completely salt-free conditions do not exist in real soils anywhere). In the salt exclusion and combined model, the effect of adding more salt is to increase the amount of freezing point depression progressively.

The three alternative models were tested against our observed SFCs. In all cases, we found that the capillary model (GCE) significantly under-predicted freezing point depression (that is, the temperature for a given liquid water content is under-predicted, or equivalently, the liquid water content for a given temperature is under-predicted). In the controlled salinity lab experiments, we found excellent agreement between the salt exclusion and combined models, with no fitting (i.e. calibration). However, for the zero salinity case, the models all failed, unless we introduced a small amount of salt. By fitting the model in this way the salt exclusion and combined models performed well. We also found that to define the SFC it was necessary to reduce the residual water content from that used in the SMC, and we speculate that this is a real phenomenon, where ice is able to propagate into smaller pores during freezing than air is during drying.

Our results suggest that, at least for the soils we considered, salt exclusion effects on freezing point depression are more important than capillary effects. The widely used GCE is likely to under-predict freezing point depression. The consequence of this is that for a given subzero temperature, the equivalent matric potential caused by freezing, as predicted by the GCE, is too low, which in coupled models is likely to lead to significant over estimates of hydraulic gradients associated with cryosuction, and associated numerical instabilities. It would be valuable in future work to explore the consequences of the salt-exclusion model in coupled models.

Acknowledgments, Samples, and Data

This project was funded by the Global Water Futures Program at the Global Institute for Water Security (GIWS) and University of Saskatchewan. We are grateful to Dr Christopher Spence from Environment and Climate Change Canada for permitting us to use his laboratory and for his feedback on this work. We thank Cody Millar from the Mine Overlay Site Testing (MOST) facility, University of Saskatchewan, for his help running some analysis on the soil. We are also grateful to Uri Nachshon and Xicai Pan for their work on the installation of the SDN field instrumentation back in 2013 and to Bruce Johnson and all the technicians at the GIWS responsible for collecting and organizing the data sets for the SDN and OJP field sites.

On acceptance of the paper, all field and lab data used will be uploaded to the Canadian Federated Research Data Repository at: https://www.frdr-dfdr.ca/repo/ and assigned a DOI number. In the meantime, the data are included in the supplementary material.

References

Azmatch, T. F., Sego, D. C., Arenson, L. U., & Biggar, K. W. (2012). Using soil freezing characteristic curve to estimate the hydraulic conductivity function of partially frozen soils. *Cold Regions Science and Technology*, *83–84*, 103–109. https://doi.org/10.1016/j.coldregions.2012.07.002

Bam, E. K. P., Brannen, R., Budhathoki, S., Ireson, A. M., & Spence, C. (2019). Meteorological, soil moisture, surface water, and groundwater data from the St. Denis National Wildlife Area, Saskatchewan, Canada. 11. *Earth System Science Data Discussions* (pp 1-21). https://doi.org/10.5194/essd-2018-125

Bam, E. K. P., & Ireson, A. M. (2019). Quantifying the wetland water balance: A new isotope-based approach that includes precipitation and infiltration. *Journal of Hydrology*, *570*, 185–200. https://doi.org/10.1016/j.jhydrol.2018.12.032

Banin, A., & Anderson, D. M. (1974). Effects of salt concentration changes during freezing on the unfrozen water Content of porous materials. *Water Resources Research*, *10*(1), 124–128. https://doi.org/10.1029/WR010i001p00124

Barr, A. G., van der Kamp, G., Black, T. A., McCaughey, J. H., & Nesic, Z. (2012). Energy balance closure at the BERMS flux towers in relation to the water balance of the White Gull Creek watershed 1999–2009. *Agricultural and Forest Meteorology*, *153*, 3–13.

Bitelli, M., Flury, M., & Campbell, G. S. (2003). A thermodielectric analyzer to measure the freezing and moisture characteristic of porous media. *Water Resources Research*, *39*(2). https://doi.org/10.1029/2001WR000930

Budhathoki, S. (2018). Modelling snowmelt infiltration processes in seasonally frozen ground [Thesis, University of Saskatchewan]. https://harvest.usask.ca/handle/10388/8468

Caicedo, B. (2017). Physical modelling of freezing and thawing of unsaturated soils. *Géotechnique*, *67*(2), 106–126. https://doi.org/10.1680/jgeot.15.P.098

Chang, C., Sommerfeldt, T. G., Carefoot, J. M., & Schaalje, G. B. (1983). Relationships of electrical conductivity with total dissolved salts and cation concentration of sulfate-dominant soil extracts. *Canadian Journal of Soil Science*, *63*(1), 79–86. https://doi.org/10.4141/cjss83-008

Christensen, A. F., He, H., Dyck, M. F., Lenore Turner, E., Chanasyk, D. S., Naeth, M. A., & Nichol, C. (2013). In situ measurement of snowmelt infiltration under various topsoil cap thicknesses on a reclaimed site. *Canadian Journal of Soil Science*, *93*(4), 497–510. https://doi.org/10.4141/cjss2012-048

Clark, M. P., Nijssen, B., Lundquist, J. D., Kavetski, D., Rupp, D. E., Woods, R. A., Freer, J. E., Gutmann, E. D., Wood, A. W., Gochis, D. J., Rasmussen, R. M., Tarboton, D. G., Mahat, V., Flerchinger, G. N., & Marks, D. G. (2015). A unified approach for process-based hydrologic modeling: 2. Model implementation and case studies. *Water Resources Research*, 51(4), 2515–2542. https://doi.org/10.1002/2015WR017200

Cuenca, R. H., Stangel, D. E., & Kelly, S. F. (1997). Soil water balance in a boreal forest. *Journal of Geophysical Research: Atmospheres*, *102*(D24), 29355–29365. https://doi.org/10.1029/97JD02312

Dall'Amico, M., Endrizzi, S., Gruber, S., & Rigon, R. (2011). A robust and energy-conserving model of freezing variably saturated soil. *The Cryosphere*, *5*(2), 469–484. https://doi.org/10.5194/tc-5-469-2011

Flerchinger, G. N., Seyfried, M. S., & Hardegree, S. P. (2006). Using soil freezing characteristics to model multi-season soil water dynamics. *Vadose Zone Journal*, *5*(4), 1143. https://doi.org/10.2136/vzj2006.0025

Francisca, F. M., & Montoro, M. A. (2012). Measuring the dielectric properties of soil–organic mixtures using coaxial impedance dielectric reflectometry. *Journal of Applied Geophysics*, *80*, 101–109. https://doi.org/10.1016/j.jappgeo.2012.01.011

Gray, D. M., & Granger, R. J. (1986). In situ measurements of moisture and salt movement in freezing soils. *Canadian Journal of Earth Sciences*, *23*(5), 696–704. https://doi.org/10.1139/e86-069

Gharedaghloo, B., Berg, S. J., & Sudicky, E. A. (2020). Water freezing characteristics in granular soils: Insights from pore-scale simulations. *Advances in Water Resources*, *143*, 103681. https://doi.org/10.1016/j.advwatres.2020.103681

Haghighi, H., Chapoy, A., & Tohidi, B. (2008). Freezing point depression of electrolyte solutions: Experimental measurements and modeling using the cubic-plus-association equation of state. *Industrial & Engineering Chemistry Research*, *47*(11), 3983–3989. https://doi.org/10.1021/ie800017e

Hayashi, M. (2013). The cold vadose zone: Hydrological and ecological significance of frozen-soil processes. *Vadose Zone Journal*, *12*(4), 1-8.

Hayashi, M., van der Kamp, G., & Rudolph, D. L. (1998). Water and solute transfer between a prairie wetland and adjacent uplands, 2. Chloride cycle. *Journal of Hydrology*, *207*(1–2), 56–67. https://doi.org/10.1016/S0022-1694(98)00099-7

He, H., Dyck, M., Zhao, Y., Si, B., Jin, H., Zhang, T., Lv, J., & Wang, J. (2016). Evaluation of five composite dielectric mixing models for understanding relationships between effective permittivity and unfrozen water content. *Cold Regions Science and Technology*, *130*, 33–42.

Hansson, K., Šimůnek, J., Mizoguchi, M., Lundin, L.-C., & Genuchten, M. T. van. (2004). Water flow and heat transport in frozen soil: Numerical solution and freeze–thaw applications. *Vadose Zone Journal*, *3*(2), 693–704. https://doi.org/10.2136/vzj2004.0693

Ireson, A. M., Barr, A. G., Johnstone, J. F., Mamet, S. D., Van Der Kamp, G., Whitfield, C. J., Michel, N. L., North, R. L., Westbrook, C. J., Debeer, C., Chun, K. P., Nazemi, A., & Sagin, J. (2015). The changing water cycle: The boreal plains ecozone of Western Canada. *Wiley Interdisciplinary Reviews: Water*, *2*(5), 505–521. https://doi.org/10.1002/wat2.1098

Kelleners, T. J., Paige, G. B., & Gray, S. T. (2009). Measurement of the Dielectric Properties of Wyoming Soils Using Electromagnetic Sensors. *Soil Science Society of America Journal*, *73*(5), 1626. https://doi.org/10.2136/sssaj2008.0361

Kelleners, T. J., & Verma, A. K. (2010). Measured and Modeled Dielectric Properties of Soils at 50 Megahertz. *Soil Science Society of America Journal*, *74*(3), 744–752. https://doi.org/10.2136/sssaj2009.0359

Kelleners, T. J., & Norton, J. B. (2012). Determining water retention in seasonally frozen soils using hydra impedance sensors. *Soil Science Society of America Journal*, *76*(1), 36. https://doi.org/10.2136/sssaj2011.0222

Koopmans, R. W. R., & Miller, R. D. (1966). Soil freezing and soil water characteristic curves. *Soil Science Society of America Journal*, *30*(6), 680–685.

Kozlowski, T. (2009). Some factors affecting supercooling and the equilibrium freezing point in soil–water systems. *Cold Regions Science and Technology*, *59*(1), 25–33. https://doi.org/10.1016/j.coldregions.2009.05.009

Kurylyk, B. L., & Watanabe, K. (2013). The mathematical representation of freezing and thawing processes in variably saturated, non-deformable soils. *Advances in Water Resources*, *60*, 160–177. https://doi.org/10.1016/j.advwatres.2013.07.016

Mizoguchi, M. (1990). Water, heat and salt transport in freezing soil [PhD thesis In Japanese, University of Tokyo, Japan].

Mohammed, A. A., Kurylyk, B. L., Cey, E. E., & Hayashi, M. (2018). Snowmelt Infiltration and macropore flow in frozen soils: Overview, knowledge gaps, and a conceptual framework. *Vadose Zone Journal*, *17*(1). https://doi.org/10.2136/vzj2018.04.0084

Nachshon, U., Ireson, A., van der Kamp, G., Davies, S. R., & Wheater, H. S. (2014). Impacts of climate variability on wetland salinization in the North American prairies. *Hydrology and Earth System Sciences*, *18*(4), 1251–1263. https://doi.org/10.5194/hess-18-1251-2014

Nazarbakhsh, M., Ireson, A. M., & Barr, A. G. (2020). Controls on evapotranspiration from jack pine forests in the Boreal Plains Ecozone. *Hydrological Processes*, *34*(4), 927–940. https://doi.org/10.1002/hyp.13674

Oquist, M. G., Sparrman, T., Klemedtsson, L., Drotz, S. H., Grip, H., Schleucher, J., & Nilsson, M. (2009). Water availability controls microbial temperature responses in frozen soil CO2 production. *Global Change Biology*, *15*(11), 2715–2722. https://doi.org/10.1111/j.1365-2486.2009.01898.x

Painter, S. L., & Karra, S. (2014). Constitutive Model for Unfrozen Water Content in Subfreezing Unsaturated Soils. Vadose Zone Journal, 13(4), vzj2013.04.0071. https://doi.org/10.2136/vzj2013.04.0071

Patterson, D. E., & Smith, M. W. (1985). Unfrozen water content in saline soils: results using time-domain reflectometry. *Canadian Geotechnical Journal*, *22*(1), 95–101.

Pekrioglu Balkis, A. (2019). Determination of SWRC for unsaturated sands, comparative study – Filter paper method versus hanging column technique. *European Journal of Science and Technology*, (16), 403–413. https://doi.org/10.31590/ejosat.539620

Pires, L. F., Brinatti, A. M., & Saab, S. da C. (2015). Experimental method to determine some physical properties in physics classes. *Revista Brasileira de Ciência Do Solo*, *39*(5), 1507–1512. https://doi.org/10.1590/01000683rbcs20140766

Ren, J., & Vanapalli, S. K. (2019). Comparison of Soil-Freezing and Soil-Water Characteristic Curves of Two Canadian Soils. *Vadose Zone Journal*, *18*(1). https://doi.org/10.2136/vzj2018.10.0185

Ren, J., & Vanapalli, S. K. (2020). Effect of freeze–thaw cycling on the soil-freezing characteristic curve of five Canadian soils. *Vadose Zone Journal*, *19*(1), e20039. https://doi.org/10.1002/vzj2.20039

Rohatgi, A. (2015). *WebPlotDigitizer User Manual Version 3.9*. 23.

Schafer, H. L., & Beier, N. A. (2017). Development of soil freezing characteristic curves for fluid fine tailings using TDR. *Geo Ottawa 2017*.

Schofield, R. K. (1935). The pF of the water in soil. *Third International Congress of Soil Science*, *2*, 37–48.

Seyfried, M. S., & Murdock, M. D. (2004). Measurement of soil water content with a 50-MHz soil dielectric sensor. *Soil Science Society of America Journal*, *68*(2), 394–403. https://doi.org/10.2136/sssaj2004.3940

Spaans, E. J. A. (1994). The soil freezing characteristic: Its measurement and similarity to the soil moisture characteristic [PhD thesis]. University of Michigan.

Spaans, E. J. A., & Baker, J. M. (1995). Examining the use of time domain reflectometry for measuring liquid water content in frozen soil. *Water Resources Research*, *31*(12), 2917–2925. https://doi.org/10.1029/95WR02769

Spaans, E. J. A., & Baker, J. M. (1996). The soil freezing characteristic: Its measurement and similarity to the soil moisture characteristic. *Soil Sci. Soc. Am. J.*, *60*, 13–19.

Stähli, M., & Stadler, D. (1997). Measurement of water and solute dynamics in freezing soil columns with time domain reflectometry. *Journal of Hydrology*, *195*(1), 352–369. https://doi.org/10.1016/S0022-1694(96)03227-1

Stevens Water Monitoring Systems Inc.: The Hydra Probe® Soil Sensor, User's Manual, 1–63, July 2007.

Susha Lekshmi, S. U., Singh, D. N., & Shojaei Baghini, M. (2014). A critical review of soil moisture measurement. *Measurement*, *54*, 92–105. https://doi.org/10.1016/j.measurement.2014.04.007

Teng, J. (2020). Parameterization of soil freezing characteristic curve for unsaturated soils. *Cold Regions Science and Technology*, 8.

Tian, Z., Ren, T., Kojima, Y., Lu, Y., Horton, R., & Heitman, J. L. (2017). An improved thermo-time domain reflectometry method for determination of ice contents in partially frozen soils. *Journal of Hydrology*, *555*, 786–796. https://doi.org/10.1016/j.jhydrol.2017.10.055

Tian, H., Wei, C., Lai, Y., & Chen, P. (2018). Quantification of Water Content during Freeze–Thaw Cycles: A Nuclear Magnetic Resonance Based Method. *Vadose Zone Journal*, *17*(1), 160124. https://doi.org/10.2136/vzj2016.12.0124

Tice, A. R., Black, P. B., & Berg, R. L. (1989). Unfrozen water contents of undisturbed and remolded Alaskan silt. *Cold Regions Science and Technology*, *17*(2), 103–111. https://doi.org/10.1016/S0165-232X(89)80001-1

Tice, A. R., Oliphant, J., Nakano, Y., & Jenkins, T. F. (1982). Relationship between the Ice and Unfrozen Water Phases in Frozen Soil as Determined by Pulsed Nuclear Magnetic Resonance and Physical Desorption Data. US Army Corps of Engineers, CRREL Report 82-15.

UMS (2015): Manual HYPROP, version 2015-01, 99 pp. UMS GmbH, Gmunder Strabe 37 Munich, Germany. http://ums-muc.de/static/Manual_HYPROP.pd

van Genuchten, M. (1980). A closed-form equation for predicting the hydraulic conductivity of unsaturated soils 1. *Soil Science Society of America Journal*, *44*(5), 892–898. https://doi.org/10.2136/sssaj1980.03615995004400050002x

Watanabe, K., Kito, T., Wake, T., & Sakai, M. (2011). Freezing experiments on unsaturated sand, loam and silt loam. *Annals of Glaciology*, *52*(58), 37–43. https://doi.org/10.3189/172756411797252220

Watanabe, K., & Mizoguchi, M. (2002). Amount of unfrozen water in frozen porous media saturated with solution. *Cold Regions Science and Technology*, *34*(2), 103–110. https://doi.org/10.1016/S0165-232X(01)00063-5

780 Watanabe, K., & Osada, Y. (2017). Simultaneous measurement of unfrozen water content and hydraulic
781 conductivity of partially frozen soil near 0 °C. *Cold Regions Science and Technology*, *142*, 79–84.
782 https://doi.org/10.1016/j.coldregions.2017.08.002

783 Watanabe, K., & Wake, T. (2009). Measurement of unfrozen water content and relative permittivity of frozen
784 unsaturated soil using NMR and TDR. *Cold Regions Science and Technology*, *59*(1), 34–41. https://doi.org/10.1016/
785 j.coldregions.2009.05.011

786 Wen, Z., Ma, W., Feng, W., Deng, Y., Wang, D., Fan, Z., & Zhou, C. (2012). Experimental study on unfrozen water
787 content and soil matric potential of Qinghai-Tibetan silty clay. *Environmental Earth Sciences*, *66*(5), 1467–1476.
788 https://doi.org/10.1007/s12665-011-1386-0

789 Williams, P. J., & Smith, M. W. (1989). The frozen earth. Cambridge University Press.

790 Williams, P. J. (1970). Properties and behaviour of freezing soils. *Norwegian Geotechnical Institute*, *72*.

791 Williams, P. J. (1964). Unfrozen water content of frozen soils and soil moisture suction. *Géotechnique*, *14*(3), 231–
792 246. https://doi.org/10.1680/geot.1964.14.3.231

793 Yan, G., Li, Z., Bore, T., Scheuermann, A., Galindo-Torres, S., & Li, L. (2017). The measurement of primary
794 drainage curve using hanging column and large soil column test. ResearchGate.
795 https://www.researchgate.net/publication/318734619

796 Yao, Y.-S., Zheng, J.-L., Chen, Z.-S., Zhang, J.-H., & Li, Y. (2016). Field measurements and numerical simulations
797 of temperature and moisture in highway engineering using a frequency domain reflectometry sensor. *Sensors (Basel,*
798 *Switzerland)*, *16*(6). https://doi.org/10.3390/s16060857

799 Yoshikawa, K., & Overduin, P. P. (2005). Comparing unfrozen water content measurements of frozen soil using
800 recently developed commercial sensors. *Cold Regions Science and Technology*, *42*(3), 250–256.
801 https://doi.org/10.1016/j.coldregions.2005.03.001

802 Zhang, C., & Liu, Z. (2018). Freezing of water confined in porous materials: role of adsorption and unfreezable
803 threshold. *Acta Geotechnica*, *13*(5), 1203–1213. https://doi.org/10.1007/s11440-018-0637-6

804 Zhou, J., Wei, C., Lai, Y., Wei, H., & Tian, H. (2018). Application of the generalized clapeyron equation to freezing
805 point depression and unfrozen water content. *Water Resources Research*, *54*(11), 9412–9431.
806 https://doi.org/10.1029/2018WR023221

807 Zhou, J., Meng, X., Wei, C., & Pei, W. (2020). Unified soil freezing characteristic for variably-saturated saline soils.
808 *Water Resources Research*, *56*(7), e2019WR026648. https://doi.org/10.1029/2019WR026648

809 Zhou, X., Zhou, J., Kinzelbach, W., & Stauffer, F. (2014). Simultaneous measurement of unfrozen water content
810 and ice content in frozen soil using gamma ray attenuation and TDR. *Water Resources Research*, *50*(12), 9630–
811 9655. https://doi.org/10.1002/2014WR015